

Flexible Dynamic Sun Tracking System (STS) Employing Machine Vision Control Approach

Franch Maverick A. Lorilla*[‡] , Renyl B. Barroca ** 

*Department of Energy Systems Management, College of Technology, University of Science and Technology of Southern Philippines, Cagayan de Oro, Philippines, 9000

**Ateneo de Davao University, Davao City, Davao del Sur, Philippines 8000

(fmalorilla@addu.edu.ph, rbbarroca@addu.edu.ph)

[‡] Corresponding Author; Franch Maverick Lorilla, 8000, Tel: +63829096288227,

fmalorilla@addu.edu.ph

Received: 05.04.2022 Accepted: 26.04.2022

Abstract- In this study, a machine vision control approach for a sun tracking system (STS) is designed, implemented, and performance is evaluated. The aim is to dynamically track the sun's centroid with high flexibility under low irradiation conditions due to weather conditions such as cloud cover. The STS is designed to work independently in the absence of a manual setup of the location's spatiotemporal data. The prototype used a 180° FOV high-resolution camera as the primary sensor for accurate image processing and adaptive control technique to regulate electrical signals to the two servo motors (pan and tilt). The NVIDIA Jetson AI-Computing Board is used for the autonomous deployment of the tracker. It was shown in the measurement that the sun's centroid tracking accuracy of the proposed tracker for Az (γ) and Al (α) is 0.23° and 0.66°, respectively, with the Solar Position Algorithm (SPA) while 0.59° and 0.65°, respectively with the commercial solar tracker, STR-22G. The results graphically and statistically show that the prototype using machine vision can measure accurately and has the same tracking performance as compared with the two established measurements. The STS application based on machine vision control approach can meet the requirements for a dynamic and flexible control system for designed Parabolic Dish Solar Concentrators.

Keywords Renewable Energy, Computer Vision, Machine Vision, Image processing, Solar Tracking System, Parabolic Concentrated solar technology

1. Introduction

One of the emerging technologies which have exhibited significant advances in energy harvesting is Concentrated Solar Power (CSP) [1]. By concentrating the sunrays in a reduced area, CSP systems can attain very high temperatures [2]. For all practical purposes, CSP using Parabolic Dish Solar Collectors (PDSC) displays a maximum of approximately 25% efficiency in converting solar energy to electricity [3], [4]. PDSC system is CSP comprised of a paraboloid-shaped reflector, a support structure, a receiver, and a STS. The entire sun irradiation that impacts the parabolic dish is reflected towards its focus, where the receiver is placed. This energy concentration allows the PDSCs to achieve temperatures as high as 1500 °C [2], [5].

While this technology is not applied in industry, a residential application holds a promise. The key reason for PDSC's potential is the excellent thermal-to-electricity performance ratio, which is almost the same as the demands placed on a domestic-use appliance, and their relatively low noise and pollution (Ferreira et al., 2015). Over the past decade, its implementation is restricted to prototypes of 10 - 100kW capacity[6].

The technology's maturity is yet to be explored since the traditional option for an efficient but costly energy source is a Photovoltaic system. Therefore, finding another reliable, safe, and cheaper energy source to reach off-grid/remote

communities is a critical challenge to address. Interestingly, there has been an increase in the market for economically sound solutions in the various stages of solar dish concentrators [7].

To raise solar concentrators' performance and make their implementation viable, many scientists and engineers have studied solar energy systems' efficiency [8][9]. In CSP technologies, STS is an essential part of improving the overall energy production. Experiments also show that tracking one or two axes can generate 20-50% more electricity than those with a fixed structure [10]. STS is accounted for about a 20% reduction of the operational costs for CSP plants [11]–[13].

However, some problems such as energy usage, reliability, weather, and maintenance also emerge and limit the solar tracker's benefits [14]. Many authors have explored the recent use of low-cost and high-quality cameras for sun tracking applications. Due to the mature technology of image sensors and more computing power become more available in smaller packages, it is increasingly running to artificial intelligence (AI) and machine learning (ML) as a control approach for an autonomous STS. Good results could be obtained through new control methods focused on AI and machine vision (MV), according to Carballo et al. (2019). This should address critical factors for a solar collector, such as block shadow and cloud detections. In their study, CSP using heliostat and parabolic trough were implemented. Thus, an opportunity to prove its functionality to PDSC would be one of this study's main interests.

Authors like Sohag et al. (2016) used either LDR or web camera mode to acquire the solar position. Control approach is based on the grayscale conversion and segmentation techniques to detect and estimate Sun's centroid. It was also proposed that it can work with the PLC to control hundreds of Photovoltaic solar panels simultaneously through the device. Lee et al. (2013) used the Cassegrain telescope to enlarge Sun's image and reduce the radiation that might cause noises on the captured image. The control strategy is based on converting the full-color image into a defined level of Hue, saturation, and light (HSL) that will result in good image binarization. Once the image is binarized, the Sobel Method is implemented to recognize Sun's boundary and 3-point formula is used to estimate the Sun's centroid correctly. The tracking algorithm is tested and established by setting up a laboratory for a sun image simulator and the STS with an image-based sun position sensor and tracking controller. It was evaluated that the proposed system can come up with 0.040o accuracy with a window setting of 5 pixels. Also, Garcia-Gil & Ramirez, (2019) used a fisheye camera with a 180 angle view to generate a panoramic image where a digital estimate of azimuth and elevation angles is reflected. Using accelerometer with a gyroscope, true north is set to correct the orientation of the angles. The captured RGB image is converted to grayscale, and 256 grays for segmentation where black is set to 0 and white is set to 256. Centroid is estimated once the brightest portion of the image is located.

Center is estimated by simply dividing both axes by 2. The center of the camera should match the center coordinate of the Sun's image by continually moving the pan and tilt motors until it stops.

Based on the literature, the study's main objective is to develop a machine vision control approach for the proposed STS using a high-resolution 180° FOV camera for accurate centroid estimation and the adoption of dynamic and flexible algorithms in image processing. Apart from other studies, the tracking performance of the proposed tracker is validated using a commercial STS, the STR-22G [19], and data from the National Renewable Energy Laboratory (NREL) using the established Solar Position Algorithm (SPA) which has the highest accuracy and error less than 0.1187695°[20], [21]

2. Methodology

2.1. System Architecture

Figure 1 illustrates the complete system architecture. It is comprised of three main components:

- Data acquisition unit - setup into three parts: built-in GPS module, gyroscope with accelerometer, and image sensor.
- Control unit - composed of a computing board and servo motor drivers
- Mechanical unit - dual-axis (azimuth-altitude) mechanism consisting of servo motors.

The system works as follows. The tracker operation starts by acquiring spatiotemporal data (date, time, latitude, and longitude of the location) of the experimental site through a built-in GPS module. The accelerometer with gyroscope (MPU-6050) will properly orient initial azimuth and altitude position with respect to true north. The solar position's data acquisition stage is completed through a 180o angle view image sensor (Sony IMX219) with an operating temperature of -20°C to +60°C and the ability to detect 3280 x 2464 resolution colors for better tracing efficiency.

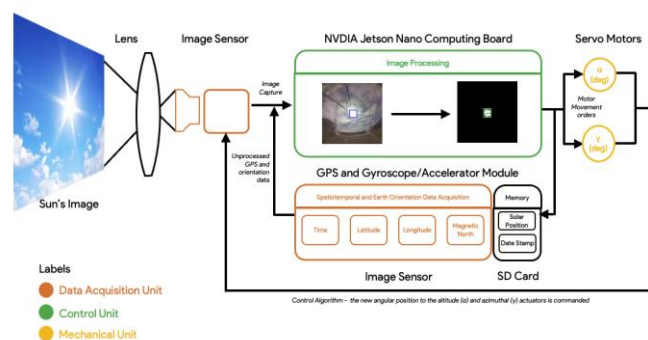







Fig. 1. System Architecture

The computing and control unit used is NVIDIA Jetson Nano, a single computing board based on a quad core ARM Cortex A57 running at 1.43 GHz and 4 GB low-power DDR4 and a 128-core GPU capable of performing 472

Billion computations/operations per seconds while only consuming 5-10W of power. Retailing from 99 USD, this board is a machine learning powerhouse and suitable for the study’s interest. The GPS, accelerator, gyroscope, and the motor drivers for servo motors (pan-tilt) were connected to

the NVIDIA Jetson. The entire image processing and algorithm to determine and record Sun’s position in real-time were implemented in Open-Source Computer Vision (OpenCV) using Python programming language via NVIDIA Jetson. Table 1 covers components used in the study.

Table 1. Summary of components used and their detailed specification

Component	Specifications	Details	Image
Sony IMX219 image sensor	Camera Pixel	8 Megapixels	
	Chip	Sony IMX219	
	Assembly Technique	SMT (ROSH)	
	Resolution	3280 × 2464	
	Pixel Size	1.12µm x1.12µm	
	Field-of-View	200°	
	Price	1,380 PHP ≈ 27 USD	
NVIDIA Jetson Nano Development Kit-B01	GPU	128-core Maxwell	
	CPU	Quad-core ARM A57 @ 1.43 GHz	
	Memory	4 GB 64-bit LPDDR4 25.6 GB/s	
	Power	5-10 W	
	Price	5,818.75 PHP ≈ 99 USD	
MG90S MicroServo	Operating Voltage	4.8 to 6V	
	Operating Speed @6.0V No load	0.10sec / 60 degrees	
	Price	563 PHP ≈ 11.26 USD	
16-Channel 12-bit PWM Servo Shield I2C Interface	Operating Voltage	3-5 V	
	Frequency	40-1000 Hz	
	No. of Channels	16	
	Resolution	12 Bits	
MPU-6050, 3-Axis Accelerometer & Gyro	Price	250 ≈ 5 USD	
	Operating Voltage	3-5 V	
	Gyro range	+ 250, 500, 1000, 2000 °/s	
	Acceleration range	± 2, ± 4, ± 8, ± 16 g	
Price:	2.5 USD		

2.2 Machine Vision

image that can exclude other objects and unavoidable noises for more accurate tracking. Figure 2 presents the steps in estimating the centroid of the captured Sun’s image.

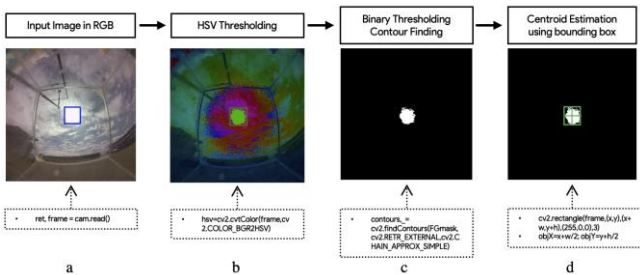


Fig. 2. Image Processing Steps

Machine vision is implemented using image processing algorithms to process, analyze, and identify sun images and their centroid. The goal is to obtain a pure and clear Sun

- a) *Full-Color Image Capture.* The image sensor dynamically tracks the Sun’s image in a 180o angle view, as shown in Figure 2(a) with the short line of code. The image is captured in a 24-bit RGB color element combination.

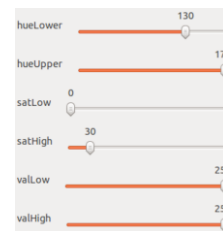


Fig. 3. HSV Dynamic tracker

b) *HSV Color Range Thresholding.* Before treating a binary image, thresholds were applied on the lowest and highest HSV or Hue value, Saturation value, and Value space to properly segment the image for better object detection, as shown in Figure 2(b) with the line of code used. At the start, it becomes tedious to try to figure out what exact values to apply; thus, GUI for track bars is provided as shown in Figure 3 to allow flexible configuration of the low and high settings of the filter. During the experimentation, the best values were set. Hue is set to 130 (low) and 179 (high). Saturation is set to 0 (low) and 30 (high). Value is set to 255 to both low and high value.

Since Sun's image is brightest in the HSV, the object that is not the brightest in the image can be separated. Saturation can be adjusted in real-time to exaggerate the difference between non-sun images such as cloud formations. The net effect is to generate more identifications without increasing false positives.

c) *Image Binarization.* To extract the Sun's bright spot, HSV conversion to black and white (binarization) is applied using a threshold which creates object masking in an image using Otsu's method shown in Figure 2(c) with the partial line of code. In this method, pixel values were analyzed to find the best balance between the two classes divided into two by minimizing the histogram's variance denoted.

The final binarized image will be cleaned further by removing the noises other than the Sun and filling in the image's holes. Figure 4 (a-b) shows different conditions of the Sun's image and its corresponding binary image.

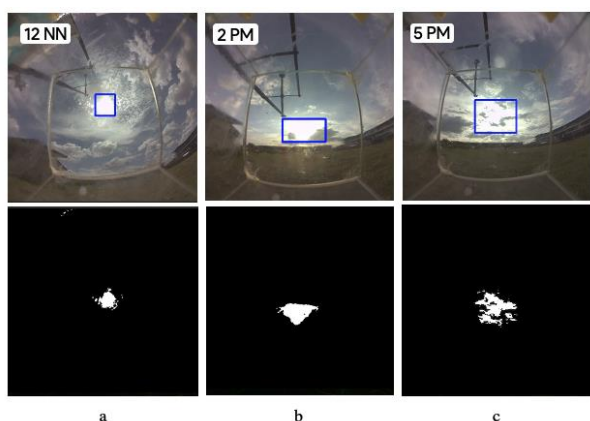


Fig. 4 Different image capture of the sky during experimental setup and calibration on April 2, 2021 with their corresponding binary output. (a) 12 Noon – no clouds; (b) 2:00 PM – fewer clouds and (c) 5:00 PM – more clouds.

d) *Sun detection and centroid estimation.* It is important to distinguish the boundary of the sun image for locating the centroid of the Sun. After identifying the largest contour, a bounding rectangle is initiated around the white spaces to quickly identify the central coordinates Sun (h,k), as shown in Figure 3(d). The intersection of

the midpoint of the bounding box dimensions is the estimated centroid.

2.3 Control Strategy and Programming

Once the centroid of the Sun (h,k) is calculated, the algorithm will match its coordinates to the centroid of the camera frame (x,y) by sending appropriate control commands to the drive motors (negative feedback). There are two main control mechanisms to understand: the Sun moves in the E/W and rises and sets in the northern and southern hemispheres (azimuthal motion and altitude motion in relation to the observer on the earth's surface). This process is repeated as the image sensor actively captures Sun's image. The results of the machine vision control approach algorithm have been shown in Figure 5.

Once initial spatiotemporal data and proper orientation of the tracker is identified and set, the image sensor starts scanning its 180° field of view for the Sun's location. Once Sun's image is detected, its central coordinates are identified, and the offset is calculated to match the camera frame's central coordinates. The calculated offset has corresponding pixel values where the motors are dynamically adjusted to correct such offset. The y-axis offset has a PWM signal that moves the servo motor in pan motion, which tracks the altitude, while the x-axis offset commands the servo motor in tilt motion, which tracks the azimuth.

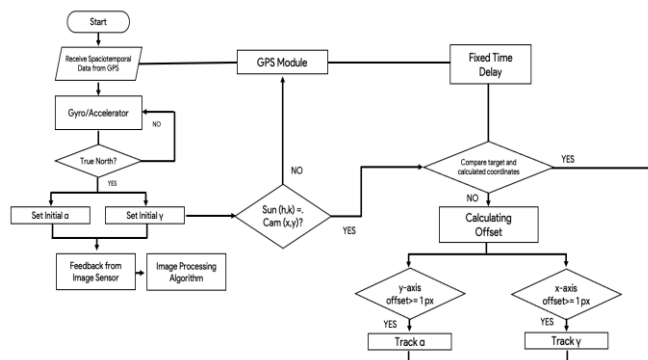


Fig. 5. Control Strategy Algorithm for dynamic-flexible motor servo operation

3. Results and Discussions

Experimental setup of the prototype is implemented at Ateneo de Davao, Bangkal, Davao City at the CSP research site (GPS: 7.0606297,125.55674). Figure 6(a) presents the close-up view of the prototype with the parts label. The image sensor's tracker arm is comprised of two servo motors that enable solar tracking in terms of altitude (α deg) and the azimuth (γ deg). The bearing is aligned in parallel with the vertical servo motor on the center end of the tracker's arm to ensure flexibility when rotated on the horizontal axis. The camera that serves as the image sensor is placed at the end of the tracker arm covered with a transparent acrylic sheet (3-mm thickness) and protective cover to filter ultraviolet and infrared wavelengths that can damage the image sensor. The solar tracker enclosure has been manufactured using the available light-yellow colored plexiglass (acrylic plastic) as it absorbs less heat and protects electronic components when subject to direct sunlight. The prototype is placed beside the

standard measuring device, STR-22G, from ECKO instruments, as seen in Figure 6(b). This device provides high tracking reliability, enhanced functionality with a fully automated setup procedure through a built-in GPS receiver. This device will serve as the primary reference data for validating the performance of the prototype.

The while prototype measures and record solar position data in real-time, STR-22G is communicating serial data every 1s via RS232c to the NVIDIA Jetson using terminal commands from the manufacturer’s manual. The data gathered from both sources were saved in CSV format. The data gathering and experimentation were conducted on April 4, 2021, from 6:00 AM to 5:30 PM. Prior to the day, weather forecasting is verified for a sunny day, and experimentation setup and calibration were arranged using Accuweather. The proponents also added reference data from NREL as

secondary reference data and as the third source of azimuth and altitude.

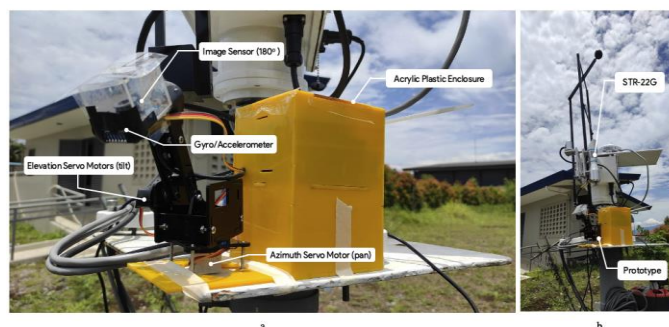


Fig. 6. (a) Developed prototype, (b) Experimental Setup of the prototype with the STR-22G Solar

Table 2. Recorded values of Azimuth (γ) and Altitude (α) in csv format.

Time (UT)	SPA Algorithm NREL		STR-22G (ADDU)		Proposed Tracker (Machine Vision)	
	γ	α	γ	α	γ	α
5.00	84.08	-0.3	83.83	0.46	83.86	-0.27
5.50	84.53	3.19	92.55	3.95	93.29	3.93
6.00	84.82	5.58	84.57	15.20	87.01	8.02
6.50	86.16	17.85	84.96	18.61	84.62	17.51
7.00	86.41	20.32	85.18	20.47	87.37	22.51
7.50	87.64	32.69	86.52	32.84	87.96	34.14
8.00	87.88	35.16	86.80	35.27	87.22	35.59
8.50	89.13	47.56	88.38	47.69	89.20	48.38
9.00	89.41	50.04	88.61	50.24	88.83	50.27
9.50	91.02	62.44	90.91	62.53	91.53	63.06
10.00	91.43	64.91	91.59	65.14	93.35	66.67
10.50	95.02	77.3	97.84	77.54	97.70	77.17
11.00	96.56	79.77	95.89	79.95	97.01	80.89
11.50	240.74	87.4	240.26	87.23	239.09	86.23
12.00	255.24	85.08	254.76	85.00	256.48	86.79
12.50	266.76	72.79	265.93	72.79	267.97	74.83
13.00	267.44	70.31	266.45	70.23	267.39	71.25
13.50	269.64	57.92	268.24	57.84	269.03	58.71
14.00	269.96	55.44	269.36	55.42	270.90	56.97
14.50	271.34	43.04	269.74	43.01	268.31	41.61
15.00	271.59	40.56	270.00	40.50	270.59	41.15
15.50	272.81	28.17	270.42	36.05	269.47	27.22
16.00	273.05	25.7	270.67	33.49	270.46	25.50
16.50	274.31	13.35	272.42	15.92	272.64	13.57
17.00	274.57	10.89	272.71	13.51	273.71	11.89
17.50	275.71	1.3	275.19	1.88	276.06	2.17

Table 2 shows the result of the recorded values of Azimuth (γ) and Altitude (α) with a specific time interval. The validation of the solar position derived from the prototype was determined through graphical comparison and statistical validation from three different source under the same condition, such as illumination and location.

Figures 7 and 8 present the graphical comparison of the three (3) sources measuring Azimuth (γ) and Altitude (α). The graph shows that the proposed system has almost the identical tracking measurement as the SPA and STR-22G.

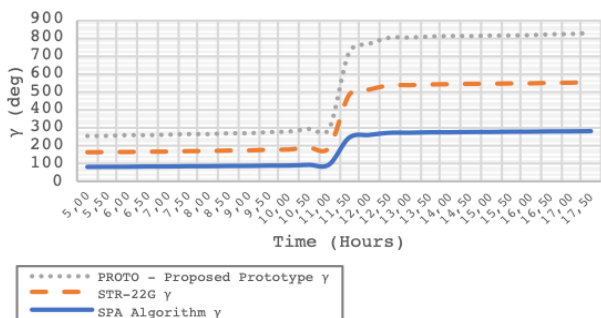


Fig 7. Graphical comparison of the 3 Sources in measuring Azimuth (γ)

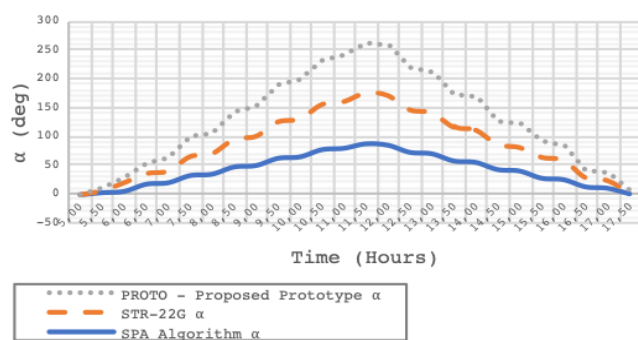


Fig 8. Graphical comparison of the 3 Sources in measuring altitude (α)

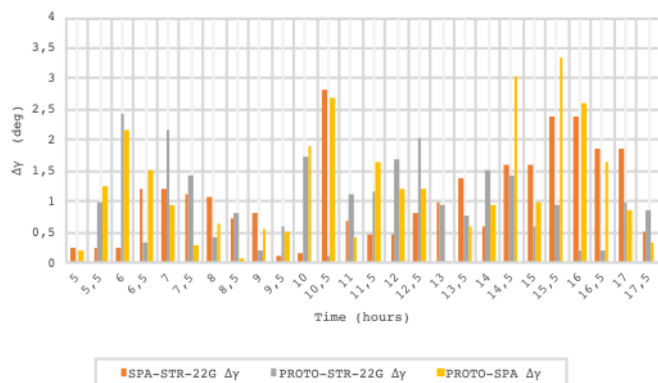


Fig. 9. Variation of Az (γ) angles of SPA and STR-22G, PROTO and STR-22G, and PROTO and SPA

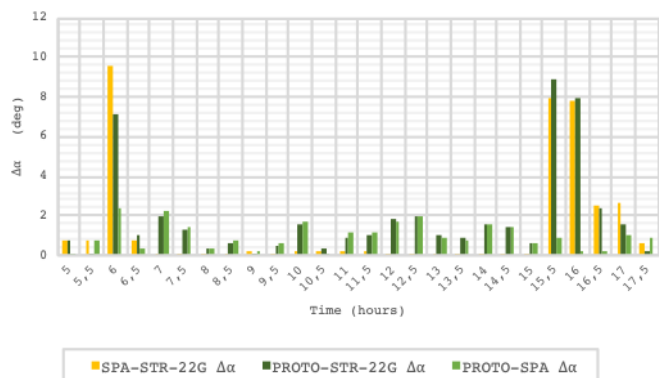


Fig. 10. Variation of Al (α) angles of SPA and STR-22G, PROTO and STR-22G, and PROTO and SPA

A one-way analysis of variance was also conducted to know if there is a significant difference on Azimuth and Elevation angles when grouped according to the sources. The Azimuth and Elevation angles were divided into three groups in terms of SPA, STR-22G, and the proposed prototype. There was no statistically significant difference as the p-value is above 0.01 on the satisfaction of the three groups: $F = 0.001$, $p = 0.999$ ($Az-\gamma$) and $F = 0.015$, $p = 0.985$ ($Al-\alpha$).

Figures 9 and 10 show that the proposed prototype has a sun's centroid measurement that could be tracked in terms of Azimuth and Altitude with an accuracy of 0.23o and 0.66o as compared with the SPA while 0.59o and 0.65 o respectively with the STR-22G. The results statistically show that the prototype using machine vision can work accurately and has the same performance as the two established measurements. With almost 150 USD total worth of prototype, this low-cost device helps present an accurate solar position measurement through a dynamic-flexible control of its servo motors.

4. Conclusions

In this paper, the design, implementation, and test of the proposed prototype are based on a machine vision control approach for a flexible-dynamic control strategy. The proposed prototype used an AI-based computing board designed for remote applications and is also composed of low-cost hardware and electronics to make the product commercially feasible in terms of price. The prototype applied all and tested of the recommendations and useful algorithms/ techniques derived from similar solar tracker studies using machine vision and image processing. One of these is the use of high-resolution cameras and the effective use of the 180o FOV to better track accuracy in finding the centroid. Different techniques in image processing and tracking customized options were adopted to make better analysis for dynamic and flexible tracking. As shown in Figure 4(b-c), the tracker can still dynamically track and locate the Sun's image's centroid under cloudy conditions.

On the other hand, a simple algorithm is also designed for motor control in work. Based on the experiment, the proposed prototype can work competitively in tracking accuracy with the commercially available solar trackers. In our future research, we intend to integrate these prototypes using Artificial Intelligence in determining the estimated value of DNI while capturing the video feed. The use of wireless control of the motors to be used in the actual CSP site. Also, it is also recommended that measured data and calculated data could be done on summer solstice, solar equinox, and winter solstice.

Acknowledgements

The researchers would like to thank the experts who were involved in the validation of this study. Without them, the researchers might not meet their objectives in doing this study. The authors would also like to acknowledge Dr. Eleonor V. Falconit, who also contributed to this study's success and the MREC-ADDU

for allowing us to access the information gathered by the STR-22G sun-tracker.

References

- [1] REN21, *Renewables 2019 Global Status Report Collaborative*, vol. 105, no. July, 2019.
- [2] J. M. L. Butti, S. Rivier, L. Delgado, S. S. Rivera, and J. E. N. McLeod, "Sun-tracking system design for parabolic dish solar concentrator," *Lect. Notes Eng. Comput. Sci.*, vol. 2236, pp. 447–452, 2018.
- [3] M. A. Soderstrand, S. B. Lee, and P. Chung, "Mini-dish based hybrid Concentrated Solar Power (CSP) system for home use," *Midwest Symp. Circuits Syst.*, pp. 689–692, 2013, doi: 10.1109/MWSCAS.2013.6674742.
- [4] Q. Chen and Y. Wang, "Research Status and Development Trend of Concentrating Solar Power," in *2020 9th International Conference on Renewable Energy Research and Application (ICRERA)*, 2020, pp. 390–393, doi: 10.1109/ICRERA49962.2020.9242893.
- [5] A. Giovannelli, "State of the art on small-scale concentrated solar power plants," *Energy Procedia*, vol. 82, pp. 607–614, 2015, doi: 10.1016/j.egypro.2015.12.008.
- [6] G. Symbolotti, "Concentrating Solar Power Technology Brief," *IEA-ETSAP and IRENA*, 2013.
- [7] F. V. Barbosa, J. L. Afonso, F. B. Rodrigues, and J. C. F. Teixeira, "Development of a solar concentrator with tracking system," *Mech. Sci.*, vol. 7, no. 2, pp. 233–245, 2016, doi: 10.5194/ms-7-233-2016.
- [8] I. Stamatescu, I. Făgărășan, G. Stamatescu, N. Arghira, and S. S. Iliescu, "Design and Implementation of a Solar-tracking Algorithm," *Procedia Eng.*, vol. 69, pp. 500–507, 2014, doi: <https://doi.org/10.1016/j.proeng.2014.03.018>.
- [9] A. Varghese, A. M. Vasanthakumary, J. Freeman, and K. Achuthan, "Remote triggered solar energy assessment using a pyrheliometer and a pyranometer," *2017 6th Int. Conf. Renew. Energy Res. Appl. ICRERA 2017*, vol. 2017-January, pp. 115–120, 2017, doi: 10.1109/ICRERA.2017.8191251.
- [10] K. E. N'Tsoukpoe, H. Liu, N. Le Pierrès, and L. Luo, "A review on long-term sorption solar energy storage," *Renew. Sustain. Energy Rev.*, vol. 13, no. 9, pp. 2385–2396, 2009, doi: <https://doi.org/10.1016/j.rser.2009.05.008>.
- [11] H. Mousazadeh, A. Keyhani, A. Javadi, H. Mobli, K. Abrinia, and A. Sharifi, "A review of principle and sun-tracking methods for maximizing solar systems output," *Renew. Sustain. Energy Rev.*, vol. 13, no. 8, pp. 1800–1818, 2009, doi: 10.1016/j.rser.2009.01.022.
- [12] P. Roth, A. Georgiev, and H. Boudinov, "Design and construction of a system for sun-tracking," *Renew. Energy*, vol. 29, no. 3, pp. 393–402, 2004, doi: [https://doi.org/10.1016/S0960-1481\(03\)00196-4](https://doi.org/10.1016/S0960-1481(03)00196-4).
- [13] G. C. Bakos, "Design and construction of a two-axis Sun tracking system for parabolic trough collector (PTC) efficiency improvement," *Renew. Energy*, vol. 31, no. 15, pp. 2411–2421, 2006, doi: <https://doi.org/10.1016/j.renene.2005.11.008>.
- [14] C. C. Wei, Y. C. Song, C. C. Chang, and C. B. Lin, "Design of a solar tracking system using the brightest region in the sky image sensor," *Sensors (Switzerland)*, vol. 16, no. 12, pp. 1–11, 2016, doi: 10.3390/s16121995.
- [15] J. A. Carballo, J. Bonilla, M. Berenguel, J. Fernández-Reche, and G. García, "Machine learning for solar trackers," *AIP Conf. Proc.*, vol. 2126, no. July, 2019, doi: 10.1063/1.5117524.
- [16] H. A. Sohag, M. Hasan, M. Khatun, and M. Ahmad, "An accurate and efficient solar tracking system using image processing and LDR sensor," *2nd Int. Conf. Electr. Inf. Commun. Technol. EICT 2015*, no. Eict, pp. 522–527, 2016, doi: 10.1109/EICT.2015.7392008.
- [17] C. D. Lee, H. C. Huang, and H. Y. Yeh, "The development of sun-tracking system using image processing," *Sensors (Switzerland)*, vol. 13, no. 5, pp. 5448–5459, 2013, doi: 10.3390/s130505448.
- [18] G. Garcia-Gil and J. M. Ramirez, "Fish-eye camera and image processing for commanding a solar tracker," *Heliyon*, vol. 5, no. 3, p. e01398, 2019, doi: 10.1016/j.heliyon.2019.e01398.
- [19] Ecko Instruments, *STR-22G Sun Trackers*. Tokyo, 2012.
- [20] I. Reda and A. Andreas, "SPA: Solar Position Algorithm," *Astrophysics Source Code Library*. p. ascl:1504.002, Apr. 01, 2015, [Online]. Available: <https://ui.adsabs.harvard.edu/abs/2015ascl.soft04002R>.
- [21] K. B. de Melo, M. Kitayama, L. R. Tavares, H. A. de Freitas, and M. G. Villalva, "Accuracy Analysis of Sun Position Calculation Algorithms: Ineichen and SPA," in *2019 IEEE PES Innovative Smart Grid Technologies Conference - Latin America (ISGT Latin America)*, 2019, pp. 1–5, doi: 10.1109/ISGT-LA.2019.8895282.